Computation of stable wrench-feasible workspace of cable-driven n-X tensegrity manipulators

Vimalesh Muralidharan, Philippe Wenger, Christine Chevallereau

Computation of stable wrench-feasible workspace of cable-driven n-X tensegrity manipulators

Vimalesh Muralidharan, Philippe Wenger, Christine Chevallereau

Laboratoire des Sciences du Numérique de Nantes (LS2N), CNRS, 44321 Nantes, France
{Vimalesh.Muralidharan, Philippe.Wenger, Christine.Chevallereau}@ls2n.fr

Résumé :

L'espace de travail stable et réalisable (SWFW) d'un manipulateur de tenségrité actionné par câble définit l'ensemble de toutes les poses de l'effecteur final atteignables avec une configuration d'équilibre stable, pour un ensemble de forces positives et bornées dans les câbles. Cet article présente une méthode efficace de calcul pour déterminer la limite du SWFW pour des manipulateurs en série cinématiquement non-redondants articulés à l'aide de mécanismes de tenségrité de type anti-parallélogramme (X). Pour un manipulateur composé de n articulations, cela implique un balayage sur $(n-1)$-dimension (D) de l'espace articulaire, à effectuer n fois, c'est-à-dire pour toutes les $\binom{n}{n-1}$ combinaisons des variables articulaires. À chaque point de la grille, un ensemble de polynômes univariés est résolu numériquement, afin de déterminer avec précision les limites de l'espace articulaire stable et réalisable (SWFJ). Ces points sont projetés dans l'espace de la tâche du manipulateur avec les singularités, pour obtenir les limites du SWFW souhaité. La méthode proposée est adaptée aux manipulateurs ayant un faible nombre d'articulations, typiquement (≤ 3). En outre, un algorithme permettant de trouver un ordre cyclique de ces points limites dans le cas d'un manipulateur à deux degrés de liberté est présenté. Cela permet d'interpoler les points limites entre eux à l'aide de segments de ligne et d'obtenir un ou plusieurs polygones se rapprochant du SWFW réel. En outre, cela facilite l'utilisation d'algorithmes existants de géométrie informatique pour inscrire un disque maximal à l'intérieur du SWFW polygonal et quantifier sa taille. Ce processus est illustré à l'aide d'un manipulateur planaire 2X entraîné par câble avec des décalages de liaison.

Abstract :

The stable wrench-feasible workspace (SWFW) of a cable-driven tensegrity manipulator defines the set of all end-effector poses reachable with a stable equilibrium configuration, for a positive and bounded input cable forces. This paper presents a computationally efficient method to determine the boundary of SWFW for kinematically non-redundant serial manipulators composed of anti-parallelogram (X) tensegrity joints. For a manipulator, composed of n joints, it involves $(n-1)$-dimensional (D) scanning of the joint space, to be performed n times, i.e., for all $\binom{n}{n-1}$ such combinations of the joint variables. At each grid point, a set of univariate polynomials are solved numerically, to determine the bounding points of stable wrench-feasible joint space (SWFJ) accurately. These points are mapped onto the task space of the manipulator along with the singularities, to obtain the boundaries of the desired SWFW. The proposed method is suitable for manipulators with low (≤ 3)-DoF. Additionally, an algorithm to find a cyclic ordering of these boundary points in the case of a 2-DoF manipulator is presented. This

allows one to interpolate between them using line segments and obtain polygon(s) approximating the actual SWFW. Further, it facilitates the use of existing algorithms from computational geometry to inscribe a maximal disk inside the polygonal SWFW and quantify its size. This process is illustrated with a cable-driven planar 2-X manipulator with link offsets.

Keywords : Tensegrity manipulator, Workspace, Wrench-feasibility, Stability

1 Introduction

Tensegrity manipulators are gaining popularity in the robotics community due to their high strength-to-weight ratio and variable stiffness properties [1]. In general, such manipulators are remotely actuated by motors placed on the base, with cables as transmission elements [2]. An important measure to quantify the performance of these manipulators is its workspace. Since these manipulators are driven by cables that can sustain only tensile forces, their reachable workspace is further qualified by the condition(s) of static equilibrium achievable with positive cable forces. When bounds on the maximum cable forces are imposed, the resulting workspace is called the wrench-feasible workspace (WFW) for a tensegrity manipulator, as defined in [3]. In this work, the WFW is further qualified by the condition of stability, to ensure that the equilibrium configurations of the manipulator are stable ones. We refer to this workspace as the stable wrench-feasible workspace (SWFW). The stability condition is useful from the control perspective, as the inherent stiffness might be sufficient to mitigate the tracking errors and produce acceptable motions with simple open-loop control laws.

In the literature, continuation methods have been employed to compute the WFW of a tensegrity manipulator [3]. However, the time taken for such computations has not been presented. A brute-force scanning technique has been followed in [4], where a 2-dimensional (D) scanning was performed in the joint space of a 2-DoF manipulator to determine the wrench-feasible joint space (WFJ) and followed by the WFW. The limitation of such a technique is that a high scanning resolution is required to obtain the boundary points with sufficient accuracy, which is a computationally expensive task. Alternatively, it is possible to derive all the limiting conditions of wrench-feasibility, stability, and joint limits, as *implicit* functions of the joint variables and plot their contours in the joint space as in [5]. But, after obtaining these plots, one needs to manually inspect one point inside each of the connected regions to find which ones are feasible and which ones are not. Though this is a viable method for analysis of a few designs, it is not suitable for a design process.

The objective of this work is to propose a computationally efficient method to determine the SWFW boundary of a kinematically non-redundant tensegrity manipulator with a *good* accuracy and in an automatic manner (i.e., without requiring human intervention). Such a method is very useful for performing a design optimization of these manipulators, where several thousand designs will be explored. It combines the accuracy of resolving implicit equations with the simplicity of scanning to achieve the goal, which comes at the cost of some tedious symbolic precomputations. For an n-DoF manipulator, it involves $(n-1)$-D scanning of the joint space to be performed n times. At each grid point, the implicit equations are converted into univariate polynomials in the remaining joint angle and solved numerically, to determine the boundary points of the stable wrench-feasible joint space (SWFJ) accurately. Then, these points are mapped onto the task space along with the singularities to obtain the SWFW.

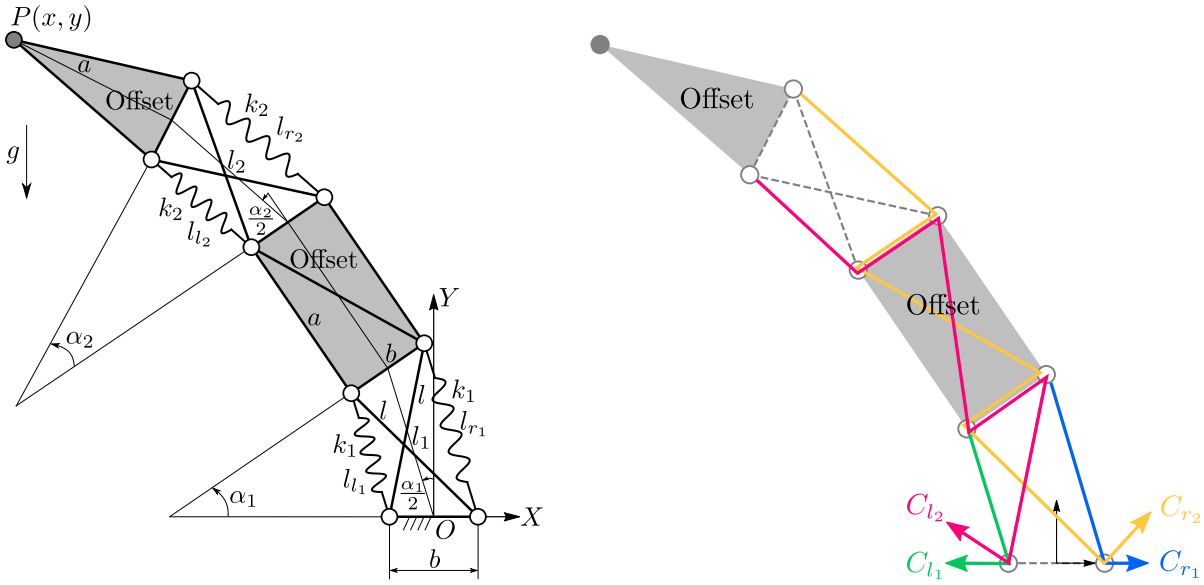

(a) Schematic (b) Actuation scheme with four cables

FIGURE 1 – Schematic diagram (left) and cable-routing scheme (right) of the 2-X manipulator with link offsets actuated by four cables.

As an illustration, the SWFW of a cable-driven 2-DoF tensegrity manipulator shown in Fig. 1 is computed using this method. The manipulator is composed of two anti-parallelogram (X) joints and link offsets. It is arranged in the vertical plane along gravity as indicated in Fig. 1a. Each joint consists of a top and base bar of length b, and two crossed bars of length l. The orientation of the top bar w.r.t. the base bar of i^{th} joint is given by α_i. Each joint is composed of identical springs with stiffness k_i on either sides, to ensure that it remains in equilibrium at $\alpha_i = 0$, in the absence of external forces. There is a rigid offset of length a between the two joints, and between the second joint and the end-effector point $P(x, y)$. This manipulator is actuated *remotely* by four motors, placed in the base, using cables $C_{l_1}, C_{r_1}, C_{l_2}, C_{r_2}$ as transmission elements, as shown in Fig. 1b. The cables C_{l_1}, C_{r_1} actuate the first joint *independently* of the second one. Likewise, the cables C_{l_2}, C_{r_2} impart movement only in the second joint as they are routed through rigid links with pulleys, in a *strut-routed* scheme [4]. The joint space of the manipulator is formed by (α_1, α_2), while the task space is formed by (x, y). Note that this manipulator is kinematically non-redundant but has an actuation redundancy of 2. For a numerical illustration, the following parameters have been adopted for the 2-X manipulator in this paper : $b = 0.05$ m, $l = 0.1$ m, $a = 0.2$ m, $k_1 = 600$ N/m, $k_2 = 300$ N/m. The forces imparted by all the cables are bounded between $F_{\min} = 5$ N and $F_{\max} = 155$ N. In this study, the springs are assumed to be of zero-free length and the pulleys to be massless points. Friction is neglected everywhere. All the bars (thick lines in Fig. 1a) are considered to be made of Aluminum material as solid cylinders of radius 0.005 m.

The rest of this paper is organized as follows. A method for computing the SWFJ is presented in Section 2. An algorithm for obtaining a cyclic ordering of the boundary points for 2-DoF manipulators is reported in Section 3, derivation of SWFW from SWFJ is addressed in Section 4. Finally, the conclusions are presented in Section 5.

2 Stable wrench-feasible joint space

Firstly, the range of motion of an X-joint is limited by the flat-singularities at $\alpha_i = \pm\pi$. Hence, for a manipulator composed of n X-joints the boundary of SWFJ must be obtained within the limits $\alpha_i \in]-\pi, \pi[\,, i = 1, \ldots, n$ in the joint space.

The condition of static equilibrium for the n-X manipulator is formed by n equations : $G_i(\alpha_1, \ldots, \alpha_n) = \Gamma_i(\alpha_i)$, for $i = 1, \ldots, n$, where G_i represents the wrench due to spring and gravity effects, and Γ_i is the wrench due to actuation cables, acting on the i^{th} joint, respectively. A method to compute G_i and Γ_i for a stack of n X-joints without offsets has been presented in [6]. It can be extended to include the link offsets by adding a few terms (see [7] for details on the model of a 2-X manipulator). Note that in Γ_i, the terms involving cable forces can vary with the cable routing, but it involves only α_i among the joint variables. The bounds on the actuation forces $[F_{\min}, F_{\max}]$ can be transferred onto the actuation wrenches as : $\Gamma_i \in [\underline{\Gamma}_i, \overline{\Gamma}_i], i = 1, \ldots, n$. Hence, using the equilibrium equations, the conditions for wrench-feasibility can be derived as : $G_i \geq \underline{\Gamma}_i$ and $G_i \leq \overline{\Gamma}_i$ for $i = 1, \ldots, n$. The limiting equations ($G_i = \underline{\Gamma}_i, G_i = \overline{\Gamma}_i$) will be considered for determining the boundary of SWFJ. Clearly, for an actuation scheme with $2n$ cables (referred to as $2n$-cable scheme), as shown in Fig. 1b, there are as many as $2n$ limiting equations obtained from the wrench-feasibility conditions. There might exist additional conditions if a cable actuates more than one joint as in the case of a side-routed scheme presented in [4].

The stability of the manipulator can be characterized by the positive-definiteness of the stiffness matrix $(\boldsymbol{K}_\alpha)_{n\times n}$, derived as the Hessian of its total potential energy w.r.t. the joint variables [4]. This matrix varies as a function of the configuration $(\alpha_1, \ldots, \alpha_n)$ as well as the force combinations that satisfy the equilibrium equations at that configuration. It is noted that the cable forces appear only on the diagonal terms of the stiffness matrix, which is evident from the functional dependence of $\Gamma_i(\alpha_i)$ only on α_i for $i = 1, \ldots, n$ in the equilibrium equations. Since it was found that the actuation forces have a positive influence on the stiffness of a single X-joint [8], it is expected that maximum stiffness be achieved at a given configuration, when maximum permissible cable forces are imposed. It follows that stable equilibrium can be achieved at this configuration only when the stiffness matrix corresponding to maximum forces is positive-definite.

For the $2n$-cable scheme, n of the redundant forces (one per joint) must be set to $F_{\max}$ to achieve maximum stiffness at any configuration. The remaining n forces can be determined from the equilibrium equations. In the i^{th} diagonal term of the stiffness matrix, one of the two antagonistic forces (F_{l_i}, F_{r_i}) actuating the i^{th} joint must be set to $F_{\max}$. However, while determining the SWFJ boundary, one does not know *a priori* which force is the critical one, hence both cases $\boldsymbol{K}_\alpha(i,i)|_{(F_{l_i}=F_{\max})}$ and $\boldsymbol{K}_\alpha(i,i)|_{(F_{r_i}=F_{\max})}$ must be considered separately, for $i = 1, \ldots, n$. Thus, in total we have 2^n possible stiffness matrices representing the upper boundary of stiffness. From each of these matrices, the limiting condition of stability (i.e., positive-definiteness) must be obtained to determine the boundary of SWFJ.

Recalling that the stiffness matrix $\boldsymbol{K}_\alpha$ is derived from the Hessian of the potential energy, it is a real symmetric matrix. Hence, it has n real eigenvalues (see [9], p. 330) and is said to be positive-definite when all eigenvalues are positive. The limiting case of positive-definiteness occurs when the least eigenvalue becomes zero, while the others remain positive. However, it is difficult to obtain explicit symbolic expressions for the eigenvalues and impose conditions on them. Hence, we use the fact that the product of eigenvalues is equal to the determinant of the matrix (see [9], p. 266) and consider $\det(\boldsymbol{K}_\alpha) = 0$

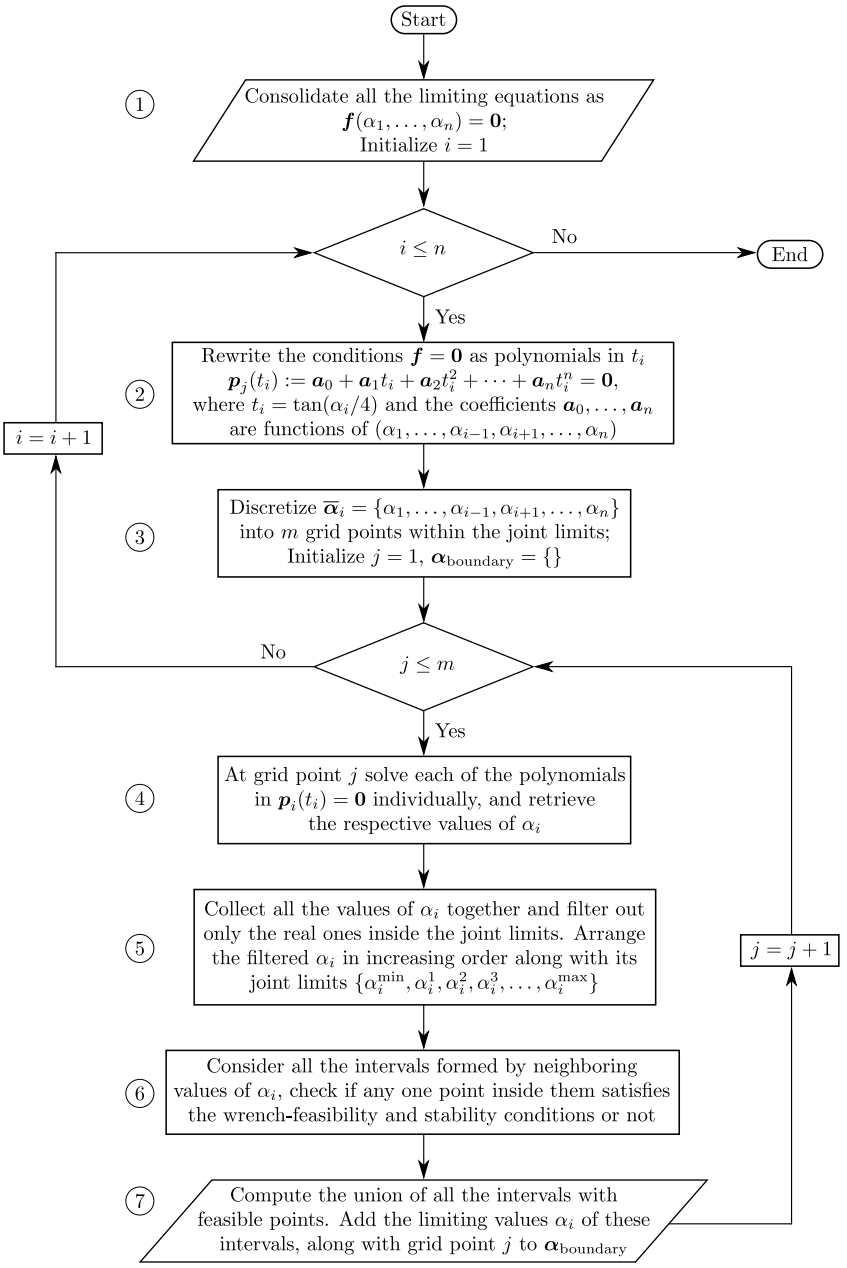

FIGURE 2 – Algorithm to compute the boundary points of a set of inequalities in the joint space.

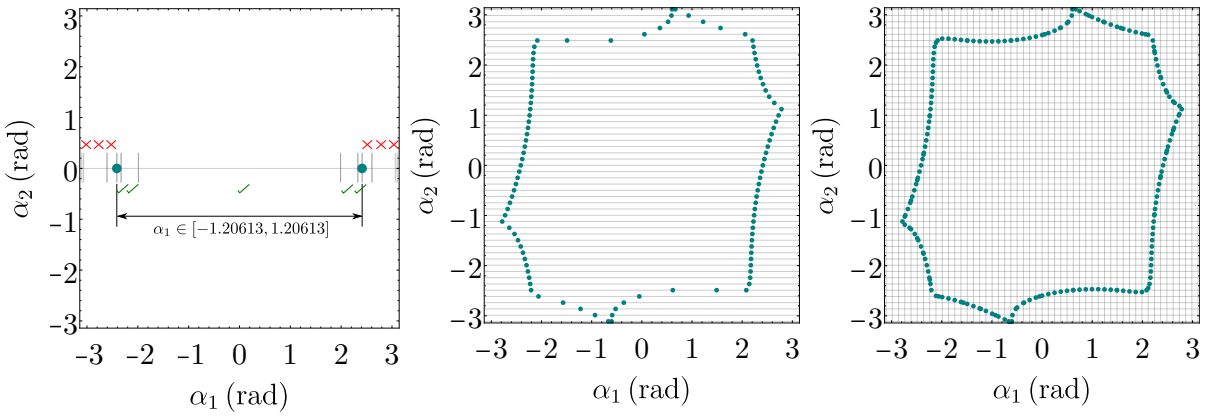

(a) Intervals of α_1 when $\alpha_2 = 0$ (b) Scanning α_2 (c) Scanning both α_1 and α_2

FIGURE 3 – 2X manipulator : Feasible interval of α_1 for a given $\alpha_2 = 0$ (left), boundary points obtained while scanning α_2 (middle), and all the boundary points obtained by scanning both α_1 and α_2 (right).

as the limiting case of stability. Clearly, it includes the vanishing of the least eigenvalue and also the vanishing of the others. But, it is possible to filter the relevant solutions from the zeros of $\det(\boldsymbol{K}_\alpha)$, by studying its neighborhood (see Fig. 3a and explanations below).

Thus, for the $2n$-cable scheme, there are $2n$ equations for wrench-feasibility and 2^n equations for stability, resulting in a total of $(2n + 2^n)$ equations for the determination of the SWFJ. Another scheme that uses $(n + 1)$ cables (referred to as $(n + 1)$-cable scheme) is also popular due to the lower number of actuators involved [10]. This scheme leads to $n(n + 1)$ equations for wrench-feasibility, and $(n + 1)$ equations for stability, respectively, resulting in a total of $(n + 1)^2$ equations.

As a first step in the determination of SWFJ, all the equations must be consolidated in a vector form as : $\boldsymbol{f} = \boldsymbol{0}$. The successive steps involved are organized into a flow chart shown in Fig. 2. The step 2 involves rewriting the limiting equations $\boldsymbol{f} = \boldsymbol{0}$ as polynomials in $t_i = \tan(\alpha_i/4)$ for $i = 1, \ldots, n$. This step is quite tedious and must be performed in symbolic form *a priori* (see [7] for more details). Since each equation must be expressed n times as polynomials in $t_1, \ldots, t_n$, respectively, for the $2n$-cable scheme $n(2n+2^n)$ polynomials must be derived, and for the $(n+1)$-cable scheme $n(n+1)^2$ polynomials must be derived. When $n = \{2, 3, 4, 5, 6\}$, this amounts to $\{16, 42, 96, 210, 456\}$ polynomials for $2n$-cable scheme and $\{18, 48, 100, 180, 294\}$ polynomials for $(n+1)$-cable scheme, respectively. Since the number of polynomials to be derived is very large for $n \geq 4$, the proposed method is practically more suitable for low ($n \leq 3$)-DoF manipulators.

For the 2-X manipulator, this method involves two 1-D scans, i.e., of α_1, α_2 variables separately. They were each discretized into 50 equally spaced points inside $[-0.99\pi, 0.99\pi]$, avoiding the flat-singularities. Steps 3-7 in the flow chart have been illustrated for the grid line $\alpha_2 = 0$ in Fig. 3a. All the roots of α_1 have been indicated with small vertical lines, and the resulting intervals were inspected for wrench-feasibility and stability with one arbitrary point (α_1^*, α_2^*) inside it. For wrench-feasibility, $(\underline{\Gamma}_i \leq G_i \leq \overline{\Gamma}_i), i = 1, 2$ were checked. For stability, firstly the two forces that can be set to $F_{\max}$ at (α_1^*, α_2^*) while respecting the bounds of remaining forces were determined. Then, all the force values and configuration (α_1^*, α_2^*) were substituted into the matrix $\boldsymbol{K}_\alpha$ and its positive-definiteness was checked. In Fig. 3a, the feasible (i.e., both wrench-feasible and stable) intervals are indicated with a tick mark, and net bounding values of α_1 are found to be $[-1.20613, 1.20613]$ radians. This process is repeated for other discrete values of α_2 in Fig. 3b and α_1 in Fig. 3c. Since the bounding points are obtained by solving polynomials, it is not possible to miss out on any of these on the grid lines. Also, they are quite accurate with a very small residue (about 10^{-10} units) w.r.t. the original conditions.

3 Cyclic ordering of SWFJ boundary points for 2-DoF manipulators

For the 2-X manipulator, an empirical method has been devised to find a cyclic ordering of the SWFJ boundary points and connect them with linear segments. This is shown as a flow chart in Fig. 5. In step 2, each of the boundary points is classified by defining four points around it, as illustrated with point A in Fig. 4a (bottom magnified part). These four points are tested for the wrench-feasibility and stability conditions, one at a time. Each of them could be either feasible or infeasible, resulting in a total of $2^4 = 16$ combinations of results. But, since we disregard the cases where all the points are either feasible or infeasible (see step 2 in Fig. 5), there are 14 possible results. Thus, every boundary point can be classified into one of the 14 categories as indicated in the last block of step 2 in Fig. 5. For the

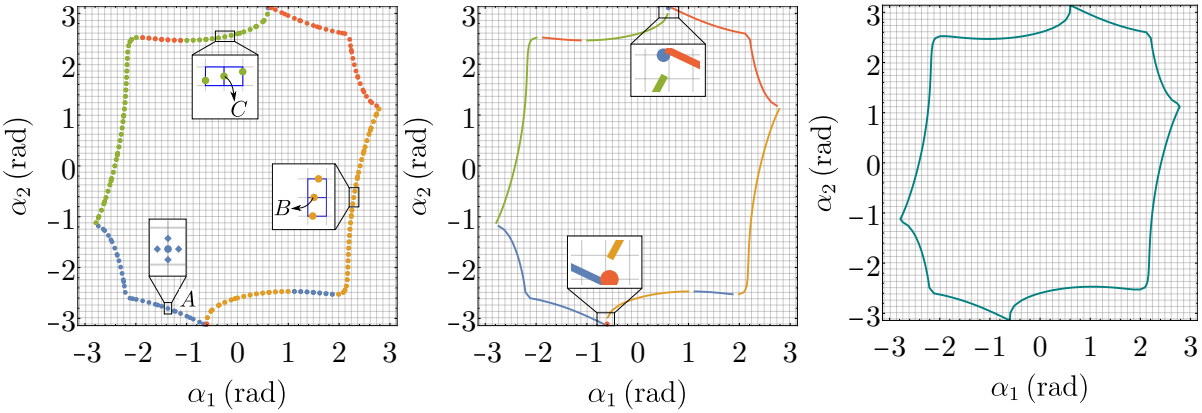

(a) Classification and grouping (b) Interpolation inside groups (c) Interpolation between groups

FIGURE 4 – 2X manipulator : Classification of boundary points into different groups (left), joining the points within groups (middle), and joining ends of the groups to form a cyclic ordering (right).

point A, only two of the four points (top and right) satisfy the wrench-feasibility and stability conditions. This case is represented by the blue color and so is point A. Similarly, when the {(top, left), (bottom, right), (bottom, left)} points are feasible, the respective boundary points are shown in {orange, green, red} colors, respectively (see Fig. 4a). In this example, it turns out that all the points belong to one of the four groups discussed above. But, in general, other groups might also exist.

The next step involves definition of rules to connect two points. Note that every point lies on either an α_2 grid line (horizontal) or an α_1 grid line (vertical). It is assumed that the boundary of SWFJ must be a continuous closed loop(s) inside the joint limits (i.e., $\alpha_1, \alpha_2 \in]-\pi, \pi[$). Thus, it follows that for any given point, its neighbor must necessarily lie on the box formed by the neighboring horizontal and vertical grid lines, or on the same grid line inside the box. For instance, consider a point B from the α_2 grid line (right magnified part of Fig. 4a), the box formed around it is highlighted by blue lines. There are two possible neighbors for this point and they are said to be *proximal* to B. Similarly, for a point C on the α_1 grid line (top magnified part of Fig. 4a), the box containing its neighbors has been defined, and there are two proximal points on it. Note that the shape of the boxes are different depending on the grid line to which the point belongs.

In step 3 (see Fig. 5), the proximal points within a group are connected starting from an open end, leading to the interpolations shown in Fig. 4b. It can be found that there are two *isolated* points that remain unconnected. Such points are treated as groups with two identical ends, and will be connected to their proximal points in step 4 (see Fig. 5), along with the other groups. This leads to a complete loop formed in Fig. 4c, which well approximates the actual SWFJ boundary. The maximum error due to the linear interpolation is limited above by the step size between two successive grid lines. One can improve the accuracy by increasing the number of grid lines.

Some other examples have been encountered where all the group ends could not be connected in step 4, due to the existence of several proximal neighbors. In such cases, the points may be connected using the minimum 2-norm condition as mentioned in steps 6 and 7 of the algorithm in Fig. 5.

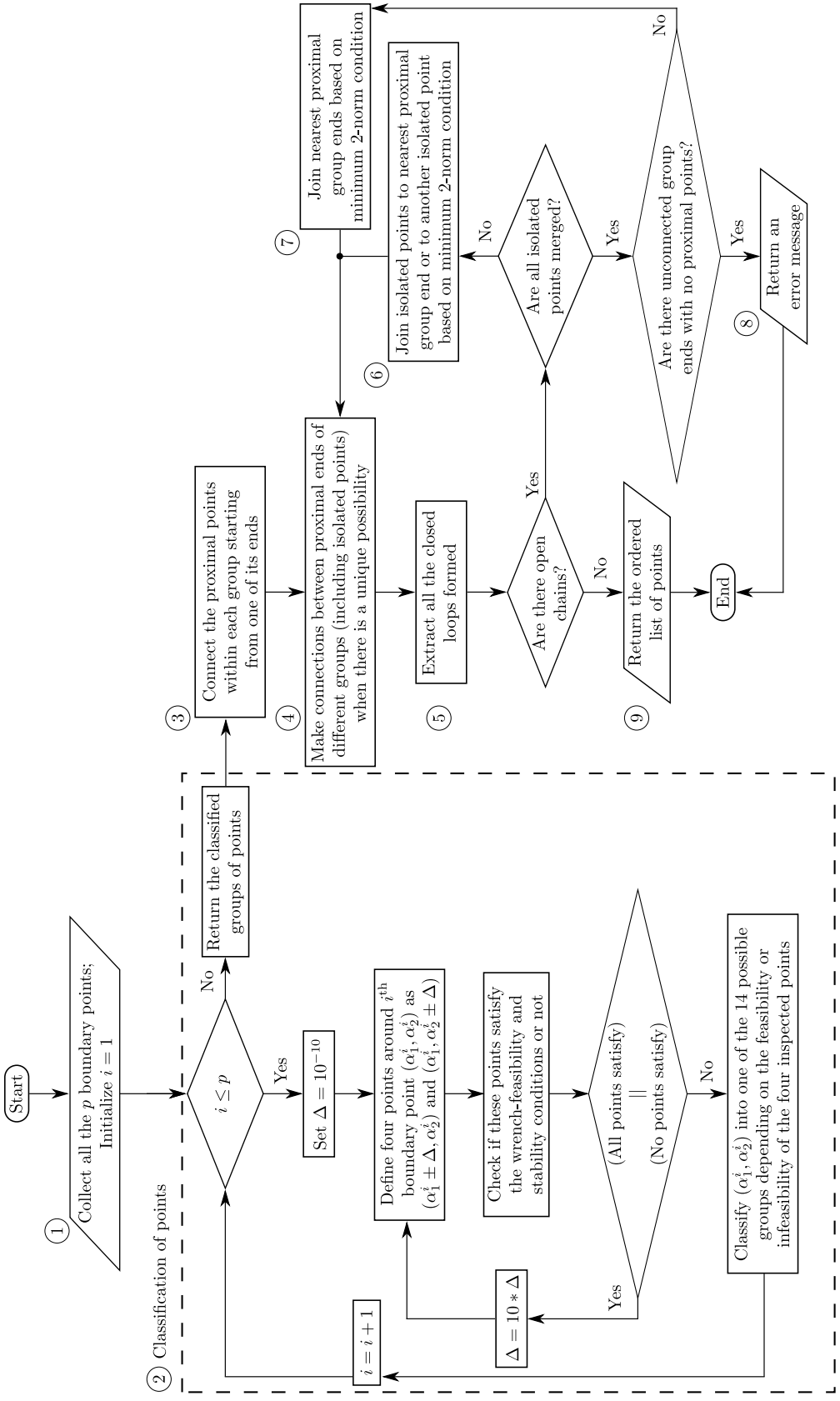

FIGURE 5 – Algorithm to find a cyclic ordering of planar points (α_1, α_2) on the boundary of the SWFI.

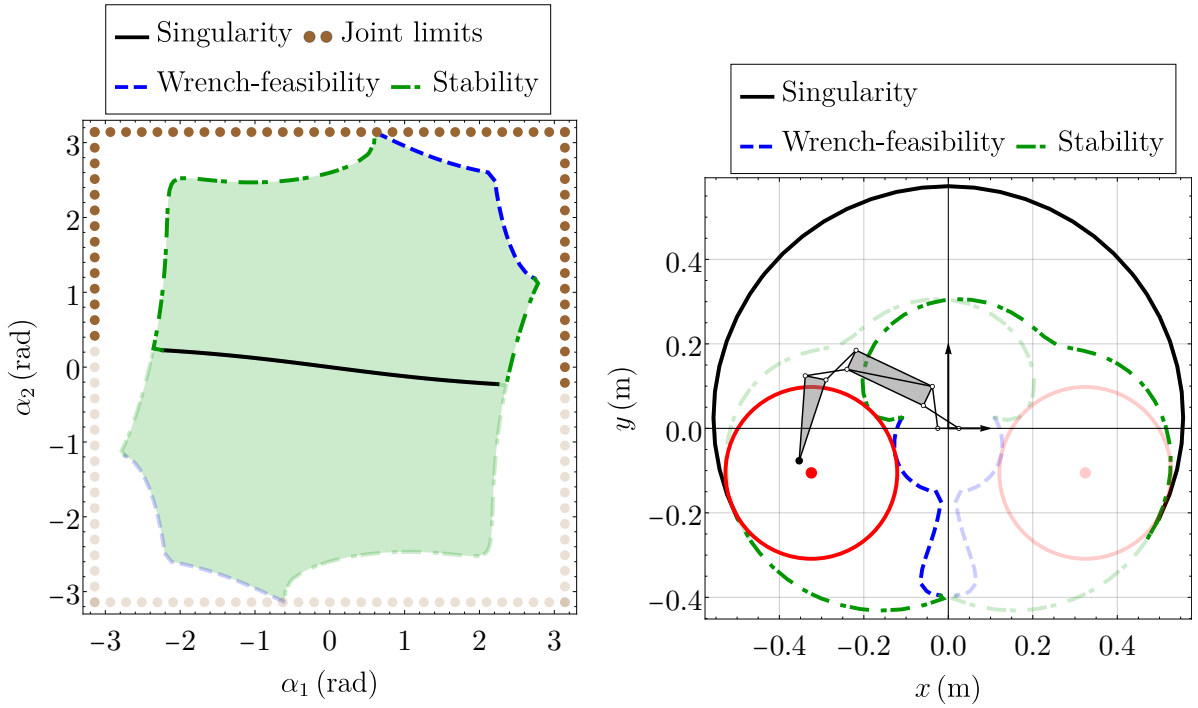

(a) Stable wrench-feasible joint space highlighted by the shaded region

(b) Stable wrench-feasible workspace with two maximally inscribed disks each of radius 0.203 m

FIGURE 6 – Stable wrench-feasible joint space (left) and stable wrench-feasible workspace (right) of the 2-X manipulator when $b = 0.05$ m, $l = 0.1$ m, $a = 0.2$ m, $k_1 = 600$ N/m, $k_2 = 300$ N/m, $F_{\max} = 155$ N, $F_{\min} = 5$ N. In joint space (α_1, α_2), the curves in region $\det(\boldsymbol{J}_x) > 0$ are shown in opaque style while those in region $\det(\boldsymbol{J}_x) < 0$ are shown in transparent style. Their maps in the task space are also shown in the same style for the sake of clarity.

4 Stable wrench-feasible workspace

The boundary of SWFJ can be mapped onto the task space of the manipulator using the direct kinematic model. Additionally, the locus of manipulator singularities inside the SWFJ must also be plotted in the task space to obtain the boundaries of the desired SWFW. For the 2-X manipulator in Fig. 1, the direct kinematics can be expressed as [11] :

$$\begin{cases} l_i(\alpha_i) = \sqrt{l^2 - b^2\cos^2(\alpha_i/2)}, \quad i = 1, 2 \\ x = -l_1(\alpha_1)\sin(\alpha_1/2) - a(\sin\alpha_1 + \sin(\alpha_1+\alpha_2)) - l_2(\alpha_2)\sin(\alpha_1+\alpha_2/2) \\ y = l_1(\alpha_1)\cos(\alpha_1/2) + a(\cos\alpha_1 + \cos(\alpha_1+\alpha_2)) + l_2(\alpha_2)\cos(\alpha_1+\alpha_2/2) \end{cases} \tag{1}$$

Differentiating Eq. (1) w.r.t. time yields :

$$\begin{bmatrix} \dot{x} \\ \dot{y} \end{bmatrix} = \boldsymbol{J}_x \begin{bmatrix} \dot{\alpha}_1 \\ \dot{\alpha}_2 \end{bmatrix}, \text{ where } \boldsymbol{J}_x = \begin{bmatrix} \frac{\partial x}{\partial \alpha_1} & \frac{\partial x}{\partial \alpha_2} \\ \frac{\partial y}{\partial \alpha_1} & \frac{\partial y}{\partial \alpha_2} \end{bmatrix} \text{ is a Jacobian matrix.} \tag{2}$$

The singularity condition is given by the vanishing of $\det(\boldsymbol{J}_x)$. The singular points in (α_1, α_2) space can also be obtained using the algorithm in Fig. 2, where $\boldsymbol{f}$ in step 1 must be replaced with $\det(\boldsymbol{J}_x)$, and the feasibility check in step 6 can be carried out w.r.t. $\det(\boldsymbol{J}_x) > 0$. The resulting points might be joined using the algorithm in Fig. 5, with the same condition $\det(\boldsymbol{J}_x) > 0$ instead of wrench-feasibility and

stability. The singularity contour and the SWFJ boundary are shown together in Fig. 6a. It is found that the singularity contour splits the SWFJ into two parts. The curves in the region $\det(\boldsymbol{J}_x) > 0$ are shown in opaque style, while those in the region $\det(\boldsymbol{J}_x) < 0$ are shown in transparent style for the sake of clarity. The bounding curves of the two parts of SWFJ are plotted in the task space to obtain the SWFW boundaries as shown in Fig. 6b. It is observed that there are two connected regions in this workspace, symmetric about $x = 0$ axis. All the points inside these regions can be reached with a stable equilibrium configuration with at least one combination of cable forces satisfying $[F_{\min}, F_{\max}]$. The intersection part in the middle can be reached with two such configurations. It is also apparent that the manipulator can be used for high stiffness tasks, e.g., machining, near the outer workspace boundary (singularity), and for low stiffness tasks, e.g., changing tool in a pallet, near the inner workspace boundary (stability limit).

Since the two parts of SWFW have been approximated as polygons, it is possible to use the `polylabel` library [1] in `c++` to fit maximally inscribed disks inside each of them, as shown in Fig. 6b. The disks are each of radius 0.203 m. The entire computation starting from the determination of boundary points to the fitting of disks takes about 91 ms (averaged over 100 runs [2]).

5 Conclusions

An algorithm is proposed for computing the stable wrench-feasible workspace (SWFW) of kinematically non-redundant cable-driven tensegrity manipulators composed of n anti-parallelogram (X) joints. It improves upon a brute-force n-dimensional (D) scanning algorithm that considers q points along each direction in the joint space, leading to an exploration of q^n grid points for the wrench-feasibility and stability conditions. However, in the proposed method, nq^{n-1} grid lines are explored in the joint space and the feasible bounds on each of the lines are determined accurately by resolving an equivalent system of polynomial equations. This improvement in accuracy and reduction in the number of explored lines over the explored points in n-D scanning, comes at the cost of tedious symbolic precomputations of the equivalent polynomials and their numerical resolution. Due to the increase in the number of polynomials with n, this method is suitable particularly for low ($n \leq 3$) degree-of-freedom manipulators, despite being applicable to the other cases. The cloud of points on the boundary of stable wrench-feasible joint space (SWFJ) can be mapped onto the task space along with the singularities to obtain an equivalent point cloud representing the boundary of SWFW.

This process has been illustrated for a 2-X manipulator with link offsets driven by four cables. Additionally, another algorithm that finds a cyclic ordering among the SWFJ boundary points for a 2-DoF manipulator has been proposed. This permits the joining of successive points with linear segments to obtain a polygonal approximation of the SWFJ and the SWFW. An existing `c++` library has been used to inscribe maximal disk(s) inside the SWFW and evaluate its size. The computation scheme is quite fast and takes only about 91 ms for the 2-X manipulator. It opens the possibility for exploring several designs of 2-X manipulator (geometry, springs, force bounds), inside an optimization framework, in a reasonable duration.

In the future, it would be useful to extend the interpolation algorithm to 3-D points, perhaps using triangulation techniques and find equivalent tools for inscribing a sphere inside the resulting polyhedron(s).

1. The associated code could be found at https://github.com/mapbox/polylabel.
2. The computations have been performed on a computer with an Intel® Core™ i7-6700 CPU running @ 3.40GHz processor, using a `C++` code.

Références

[1] Y. Liu, Q. Bi, X. Yue, J. Wu, B. Yang, Y. Li, A review on tensegrity structures-based robots, Mechanism and Machine Theory 168 (2022) 104571. doi:10.1016/j.mechmachtheory.2021.104571.

[2] F. Li, H. Peng, H. Yang, Z. Kan, A symplectic kinodynamic planning method for cable-driven tensegrity manipulators in a dynamic environment, Nonlinear Dynamics 106 (2021) 2919–2941. doi:10.1007/s11071-021-06927-w.

[3] Q. Boehler, I. Charpentier, M. S. Vedrines, P. Renaud, Definition and computation of tensegrity mechanism workspace, Journal of Mechanisms and Robotics 7 (4) (2015) 044502. doi:10.1115/1.4029809.

[4] M. Furet, P. Wenger, Kinetostatic analysis and actuation strategy of a planar tensegrity 2-X manipulator, Journal of Mechanisms and Robotics 11 (6) (2019) 060904. doi:10.1115/1.4044209.

[5] M. Arsenault, C. M. Gosselin, Kinematic, static and dynamic analysis of a planar 2-DOF tensegrity mechanism, Mechanism and Machine Theory 41 (9) (2006) 1072–1089. doi:10.1016/j.mechmachtheory.2005.10.014.

[6] B. Fasquelle, M. Furet, C. Chevallereau, P. Wenger, Dynamic modeling and control of a tensegrity manipulator mimicking a bird neck, in : T. Uhl (Ed.), Advances in Mechanism and Machine Science, Springer International Publishing, Cham, 2019, pp. 2087–2097.

[7] V. Muralidharan, Stable wrench-feasible workspace of 2-X tensegrity manipulator, Technical report, LS2N, École Centrale de Nantes (2022).

[8] V. Muralidharan, P. Wenger, Optimal design and comparative study of two antagonistically actuated tensegrity joints, Mechanism and Machine Theory 159 (2021) 104249. doi:10.1016/j.mechmachtheory.2021.104249.

[9] G. Strang, Linear Algebra and its Applications, 4th Edition, Cengage Learning India Pvt. Ltd., New Delhi, 2006.

[10] B. Fasquelle, P. Khanna, C. Chevallereau, D. Chablat, D. Creusot, S. Jolivet, P. Lemoine, P. Wenger, Identification and control of a 3-X cable-driven manipulator inspired from the bird's neck, Journal of Mechanisms and Robotics 14 (1) (2021) 011005. doi:10.1115/1.4051521.

[11] P. Wenger, M. Furet, Kinematic analysis of a planar manipulator with anti-parallelogram joints and offsets, in : J. Lenarčič, B. Siciliano (Eds.), Advances in Robot Kinematics 2020, Springer International Publishing, Cham, 2021, pp. 319–326.